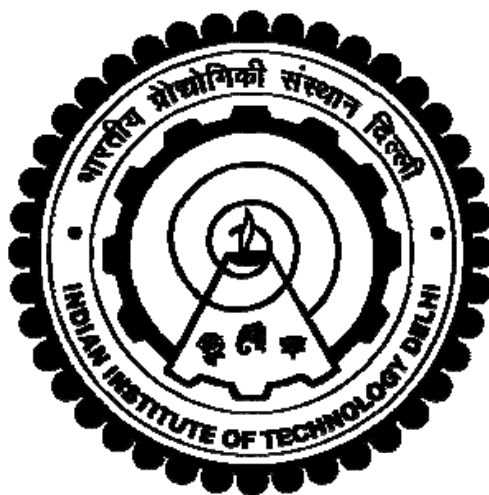


**MULTIFUNCTIONAL NANOMATERIALS AND THEIR COMPOSITES  
FOR BIOPOTENTIAL (ECG) SENSING: SYNTHESIS AND  
NANOMECHANICAL ANALYSIS**

**YOGITA MAITHANI**



**DEPARTMENT OF PHYSICS  
INDIAN INSTITUTE OF TECHNOLOGY DELHI**

**MARCH 2023**

© Indian Institute of Technology Delhi (IITD), New Delhi, 2023

**Multifunctional nanomaterials and their composites  
for biopotential (ECG) sensing: synthesis and  
nanomechanical analysis**

by

**Yogita Maithani**

**Department of Physics**

**Submitted**

**in fulfilment of the requirements of the degree of Doctor of Philosophy**

**to the**



**INDIAN INSTITUTE OF TECHNOLOGY DELHI**

**March, 2023**

This thesis is dedicated to my parents

*For their endless love, support and encouragement*

## **Certificate**

This is to certify that the thesis entitled “**Multifunctional nanomaterials and their composites for biopotential (ECG) sensing: synthesis and nanomechanical analysis**” being submitted by **Ms. Yogita Maithani** to **Indian Institute of Technology Delhi** for the award of the degree of **Doctor of Philosophy** is a record of bonafide research work carried out by her. She has worked under our guidance and supervision and has fulfilled the requirements, which to our knowledge have reached the requisite standard for the submission of the thesis.

The results contained in this thesis have not been submitted in part or full to any other University or Institute for the award of any degree or diploma.

**Date:**

**Prof J. P. Singh**

Department of Physics  
Indian Institute of Technology Delhi  
New Delhi – 110016

**Prof. B. R. Mehta**

Department of Physics  
Indian Institute of Technology Delhi,  
New Delhi – 110016

---

## Acknowledgments

---

My Ph.D. time at IIT Delhi has been challenging and enjoyable but more life-defining. I feel privileged to be thankful to the divine and the many people whose support, assistance, and encouragement have made this thesis possible.

First and foremost, I would like to express my love and gratitude to my parents, who have encouraged me to pursue my work freely and have always been there to motivate me for their blessings, unconditional love, care, support, and encouragement throughout all stages of my Ph.D. and for making me believe in myself.

This work would not have reached its present form without the guidance of my supervisors, Prof. J. P. Singh and Prof. B. R. Mehta. I would like to express my sincere gratitude to them; it has been an honor to be their student. I am grateful to them for their useful suggestions, encouragement to work on research ideas, and for providing the opportunity to do experimental work. Prof. Singh has always been open to new ideas and encouraged to attempt tasks even if they seemed difficult or impossible initially. His analytical approach has left a long-lasting impression on me. Apart from this, he is also receptive to non-academic problems that a student may face and has been supportive under such circumstances. Prof. Mehta has been a guiding light throughout my work and has given his valuable inputs at all stages. I express deep gratitude to both of them for supporting me at every stage of my work.

I would also like to thank my Ph.D. research committee members Prof. G.V. Prakash (Department of Physics), Prof. Rajesh Khanna (Department of Chemical Engineering), Prof. Saswata Bhattacharya (Department of Physics), for their timely evaluations, comments, and suggestions during research work. I would like to thank Prof. Neeraj Khare (Department of Physics) for his support. I acknowledge the department of Physics, Indian Institute of Technology Delhi, for allowing me to work here.

I express my deep gratitude towards Prof. Abhijit Majumdar (Department of Textile & Fibre Engineering, IITD), Dr. Bijit Choudhuri (NIT Silchar), Prof. Chandra Shekhar Yerramalli (Aerospace Engineering, IIT Bombay) for providing me with various inputs for my research. I also acknowledge Dr. Mukesh Bajwa, Dr. Sagar Ingle, and Dr. Bhawatosh for helping me in carrying out the experiments related to the mechanical properties of textile and their composites. I gratefully acknowledge the Nanoscale Research Facility (NRF) and Central Research Facility (CRF) at the Indian Institute of Technology Delhi for providing experimental facilities during this course of work.

I have enjoyed working all these years at IIT Delhi, where I found a healthy, comfortable, and friendly ambiance to work. Working together with lab mates, discussions both academic and non-academic, and their moral support will always be remembered. I would like to thank my seniors, Dr. Samir Kumar, Dr. Parul Raturi, Dr. Leeladhar Kaushik, Dr. Indrani Mishra, Dr. Bijit Choudhuri, Dr. Shashank Gahlaut, Dr. Pinki, Dr. Rizwin khannam, Dr. Anoop sunny, Dr. Sakshi Kpoor and my labmates, Meenu Pandey, Sarjana Yadav, Jyoti Yadav, Jamal Ahmad Khan, Rishav Sharma, Sneha Senapati, Sidharth Rana, Shivam Singh, CM Vidya, Lakshay, Nidhi, Bhawna, Rajat, Debottam for their encouragement and scientific discussions. Special thanks to Jyoti Chand (Anshul) for her constant support and for creating a pleasant environment in the lab. I also feel privileged to be associated with the Glad and nano CVD lab and Thin Film lab.

I would also like to thank my friends Shuchi Kaushik, Subhajit Karmarkar, Somyarup Hait, and Jayjit Mukherjee, who were with me at various stages throughout my Ph.D. They have always been very kind to help me with their experience in planning and tackling different things. I thank them for being with me in both good and bad times. My heart wants to say so many things to you all, but it can all be summed up in one sentence: Thank you for all of the laughs, advice, and sweet memories throughout the time.

I would also like to take this opportunity to thank my school and college teachers, who have always inspired me. I would also like to thank my friend Jaydeep Singh and my

brother Vinay Maithani for keeping me motivated toward research during my ups and downs and for many scientific discussions.

I realize the importance of not giving up, which has now culminated in the form of this thesis. I hope the readers of this thesis find the work interesting and enjoy reading it.

Thank you.

Yogita Maithani

---

## Abstract

---

Composite materials are created by mixing two or more unique materials to merge their qualities. Nanocomposite materials, which incorporate nanomaterial, can significantly improve the host material's electrical, thermal, and mechanical characteristics and have a broad range of emerging uses, including in healthcare and flexible electronics. Healthcare is one of the most significant challenges for modern civilization, especially with the world's population increasing at an alarming rate. The threat of being infected with novel microbes has also increased drastically due to our poor life style. Nanocomposites created by integrating elastic polymers and metallic nanoparticles have recently attracted the interest of human-friendly wearable electronics. Due to the inherent high-stretchable nature of the elastomers and the excellent electrical properties of the metal nanostructures, such nanocomposites have shown the potential to achieve high intrinsic stretchability and high conductivity. Stretchable conductors with excellent electrical and mechanical properties can be made by optimizing metallic nanocomposites' material design and fabrication procedures.

This study aims to develop and study the nanostructures and their smart nano-composite materials that can be used in various applications. The work will also look at the viability of making portable devices for healthcare and evaluate the mechanical and electrical characteristics of fabricated nanocomposite materials.

In the first work, a highly flexible, conductive, and self-adhesive silver nanorods (AgNRs) embedded polydimethylsiloxane (PDMS) dry electrode has been fabricated and studied for long-term electrocardiogram (ECG) monitoring. We used a unique glancing angle deposition method to fabricate AgNRs and then embedded them in a biocompatible polymer PDMS matrix. Even after several hours of use, the fabricated electrodes do not irritate the skin. These AgNRs-PDMS electrodes have an electrical resistivity of  $10^{-7} \Omega\text{-m}$  and a skin contact impedance of  $93.9 \pm 0.7 \text{ k}\Omega$  to  $6.2 \pm 3.7 \text{ k}\Omega$  for frequencies ranging from 40 Hz to 1 kHz, which is around 18% less than most conventional Ag/AgCl wet electrodes.

Further, the AgNRs were embedded in the RGO-PDMS composite matrix, which improve the nanocomposite's mechanical properties with maintaining its stretchability. The fabricated AgNRs embedded RGO-PDMS dry electrode possesses good electrical conductivity and skin contact impedance between  $70.1 \pm 0.7 \text{ k}\Omega$  to  $5.6 \pm 1.7 \text{ k}\Omega$  for frequencies ranging from 40 Hz to 1 kHz, comparable to conventional Ag/AgCl wet electrodes. These electrodes give excellent-quality ECG signals and do not cause skin irritation even after several hours of usage. They offer high skin compatibility and good signal quality, which are prominent features for cardiorespiratory monitoring. A signal acquisition circuit is designed to detect ECG signals combined with proposed dry electrodes and a wireless monitoring device. Finally, real-time ECG signals are displayed on a mobile phone via an Android application. These AgNRs embedded polymer nanocomposite-based dry electrodes, in combination with the portable wireless device, may be used in future clinical studies that require real-time and long-term ECG monitoring. We achieved comparable performance, with significantly reduced electrode-skin impedance for clinical-quality ECG recording without using gels or causing discomfort after prolonged wear.

The next work presents the special type of nanocomposites treated textiles based dry biopotential potential electrodes that have been presented for long-term ECG monitoring. The dry electrodes for biopotential sensing made by wearable textile electrodes are promising candidates for long-term health monitoring in terms of comfort to overcome the drawbacks of wet and metal electrodes. In this work, three types of textile-based electrodes are fabricated and studied for their use as a dry electrodes for ECG monitoring. The first textile electrode is a cotton-based textile dry electrode for ECG monitoring via the treatment of prepared conductive ink by Poly(3,4-ethylene dioxythiophene) (PEDOT): Poly (styrene sulfonate) (PSS) and DMSO were fabricated. The ECG is monitored by a portable self-designed low-cost Arduino-based device and validated by a standard ECG monitoring system. The second textile electrode, an AgNRs and PEDOT: PSS treated Kevlar fabric, is fabricated and studied. It shows uniform and high electrical conductivity. The electrode offers high skin compatibility and good signal quality, which are prominent

features for cardiorespiratory monitoring. Third textile electrode, PEDOT: PSS coated laser-induced graphene (LIG) Kevlar textile dry electrodes for long-term ECG monitoring. Here the direct writing of laser-induced graphene (LIG) on a Kevlar textile were used for the production of LIG Kevlar. This structure enables the incorporation of functions into the textile while retaining wear comfort. The electrode as-prepared has a high electrical conductivity and skin contact impedance of  $100 \pm 3 \text{ k}\Omega$  (at 40 Hz) to  $7.9 \pm 3.7 \text{ k}\Omega$  for frequencies ranging from 40 Hz to 1 kHz, which is around 13% less than most conventional Ag/AgCl wet electrodes. The results show comparable performance with significantly lower electrode-skin impedance for clinical quality. Even after several hours of use, these electrodes cause no skin irritation and work effectively without the need for skin preparation. The fabrication of the PEDOT: PSS-graphene/Kevlar textile electrode is simple and inexpensive, and it can be mass-produced without requiring any complex or time-consuming procedures, which benefits the practical applications of this approach.

The following work describes the fabrication and study of nanomechanical properties of nano structural materials such as AgNRs embedded polymer matrix and  $\text{ZrO}_2$  thin films using nanoindentation. Here the effect of AgNRs on the properties of the PDMS polymer matrix was studied. The surface, mechanical and electrical properties of PDMS are significantly changed after embedding the AgNRs in it. The results show that surface roughness and polarity increase after AgNRs are embedded in the PDMS matrix. Elastic modulus (E) and hardness (H) decrease with an increase in the indentation load as a result of the indentation depth effect. Due to the strong interfacial adhesion of AgNRs embedded in the PDMS matrix, the E and H of nanocomposite are increased by 167.6% and 93.3% compared with PDMS film, respectively. It remains conductive during various mechanical strains such as bending, twisting, and stretching, which is demonstrated using a light-emitting diode circuit. Simultaneously, the antimicrobial activity of silver could make it a promising candidate for wearable electronics. The results show that the electrically conducting and mechanically reliable AgNRs-PDMS composite may have the potential to be used as stretchable electrodes. Further, zirconia thin film was deposited using the e-beam evaporation technique followed by thermal annealing to optimize the cubic phase of

zirconia. This work systematically analyses the effects of annealing temperature on different properties of zirconia film, such as structural, optical, wetting, and mechanical properties. The results of nanoindentation demonstrate the impact of annealing temperature on the mechanical properties of the deposited film. The hardness and elastic modulus increased as the annealing temperature increased. The zirconia film annealed at 500°C had the cubic phase, large grain size, highest optical transmittance, hydrophilicity, hardness, and elastic modulus. As a result, the post-annealing temperature strongly influences the characteristics of zirconia film, which can provide a method for tuning the optical, wetting, and mechanical properties of the zirconia film.

In further work, the nanomechanical properties of AgNRs-coated textiles and textile epoxy composites have been investigated. The Ag nanorods were grown on the surface of para-aramid (Kevlar) fiber using the glancing angle deposition technique. The AgNRs increase inter-yarn friction, which is one of the important parameters for energy absorption applications and can be used for lightweight, soft body armor. The nanowires have a minimal effect on the flexibility of the fabric, and the amount of extra weight added to the fabric is negligible. Further, the effect of Ag nanorods on the mechanical characteristics of Kevlar-epoxy composites is explored. Following that, these hybrid composites are subjected to tensile, flexural, and low-velocity impact tests, and their performance is directly compared to that of a basic Kevlar-epoxy composite. AgNRs-treated Kevlar composites are shown to increase interlaminar and interfacial characteristics. Our findings hold promise for fabricating and studying different types of nanocomposites.

## सार

कम्पोजिट पदार्थ दो या दो से अधिक अद्वितीय पदार्थों को मिलाकर उनके गुणों को मिला कर बनाई जाती है। नैनोकम्पोजिट पदार्थ, जिसमें नैनो पदार्थ शामिल है, मेजबान सामग्री की विद्युत, थर्मल और यांत्रिक विशेषताओं में काफी सुधार कर सकती है और स्वास्थ्य देखभाल और फ्लैक्सिबल इलेक्ट्रॉनिक्स सहित उभरते उपयोगों की एक विस्तृत श्रृंखला है। स्वास्थ्य सेवा आधुनिक सभ्यता के लिए सबसे महत्वपूर्ण चुनौतियों में से एक है, विशेष रूप से दुनिया की आबादी खतरनाक दर से बढ़ रही है। हमारी खराब जीवन शैली के कारण नए रोगाणुओं से संक्रमित होने का खतरा भी काफी बढ़ गया है। फ्लैक्सिबल पॉलिमर और धातु के नैनोकणों को एकीकृत करके बनाए गए नैनोकंपोजिट्स ने हाल ही में मानव-अनुकूल पहनने योग्य इलेक्ट्रॉनिक्स के हित को आकर्षित किया है। इलास्टोमर्स की अंतर्निहित उच्च-खिंचाव प्रकृति और धातु नैनोस्ट्रक्चर के उत्कृष्ट विद्युत गुणों के कारण, ऐसे नैनोकम्पोजिट्स ने उच्च आंतरिक खिंचाव और उच्च चालकता प्राप्त करने की क्षमता दिखाई है। धात्विक नैनोकम्पोजिट्स की सामग्री डिजाइन और निर्माण प्रक्रियाओं को अनुकूलित करके उत्कृष्ट विद्युत और यांत्रिक गुणों वाले स्ट्रेचेबल कंडक्टर बनाए जा सकते हैं।

इस अध्ययन का उद्देश्य नैनोस्ट्रक्चर और उनकी स्मार्ट नैनो-मिश्रित सामग्रियों का विकास और अध्ययन करना है जिनका उपयोग विभिन्न अनुप्रयोगों में किया जा सकता है। काम स्वास्थ्य देखभाल के लिए पोर्टेबल डिवाइस बनाने की व्यवहार्यता को भी देखेगा और फैब्रिकेटेड नैनोकंपोजिट सामग्री की यांत्रिक और विद्युत विशेषताओं का मूल्यांकन करेगा।

पहले काम में, एक अत्यधिक लचीला, प्रवाहकीय, और स्वयं-चिपकने वाला चांदी नैनोरोड्स (AgNRs) एम्बेडेड पॉलीडिमिथाइलसिलोक्सेन (PDMS) शुष्क इलेक्ट्रोड को लंबे समय तक इलेक्ट्रोकार्डियोग्राम (ECG) निगरानी के लिए निर्मित और अध्ययन किया गया है। हमने AgNRs को बनाने के लिए एक अद्वितीय ग्लैसिंग एंगल डिपोजिशन विधि का उपयोग किया और फिर उन्हें एक बायोकम्पैटिबल पॉलीमर PDMS मैट्रिक्स में एम्बेड किया। कई घंटों के उपयोग के बाद भी, गढ़े हुए इलेक्ट्रोड त्वचा को परेशान नहीं करते हैं। इन AgNRs-PDMS इलेक्ट्रोड में  $10^{-7}$   $\Omega$ -m की विद्युत प्रतिरोधकता और 40 Hz से 1 kHz तक की आवृत्तियों के लिए  $93.9 \pm 0.7$  k $\Omega$  से  $6.2 \pm 3.7$  k $\Omega$  की त्वचा संपर्क प्रतिबाधा है, जो कि अधिकांश पारंपरिक Ag/AgCl गीले इलेक्ट्रोड से लगभग 18% कम है

इसके अलावा, AgNRs को RGO-PDMS कम्पोजिट मैट्रिक्स में एम्बेड किया गया था, जो नैनोकम्पोजिट के यांत्रिक गुणों में सुधार करता है और इसकी खिंचाव क्षमता को बनाए रखता है। गढ़े हुए AgNRs एम्बेडेड RGO-PDMS शुष्क इलेक्ट्रोड में 40 Hz से 1 kHz तक की आवृत्तियों के लिए  $70.1 \pm 0.7$  k $\Omega$  से  $5.6 \pm 1.7$  k $\Omega$  के बीच अच्छी विद्युत चालकता और त्वचा संपर्क प्रतिबाधा होती है, जो पारंपरिक Ag/AgCl गीले इलेक्ट्रोड के बराबर होती है। ये इलेक्ट्रोड उत्कृष्ट गुणवत्ता वाले ईसीजी संकेत देते हैं और कई घंटों के उपयोग के बाद भी त्वचा में जलन पैदा

नहीं करते हैं। वे उच्च त्वचा संगतता और अच्छी सिग्नल गुणवत्ता प्रदान करते हैं, जो कार्डियोरेस्पिरेटरी मॉनिटरिंग के लिए प्रमुख विशेषताएं हैं। एक सिग्नल अधिग्रहण सर्किट प्रस्तावित सूखे इलेक्ट्रोड और एक वायरलेस मॉनिटरिंग डिवाइस के साथ मिलकर ईसीजी सिग्नल का पता लगाने के लिए डिज़ाइन किया गया है। अंत में, रीयल-टाइम ईसीजी सिग्नल एंड्रॉइड एप्लिकेशन के माध्यम से मोबाइल फोन पर प्रदर्शित होते हैं। इन AgNRs एम्बेडेड पॉलीमर नैनोकम्पोजिट-आधारित ड्राई इलेक्ट्रोड, पोर्टेबल वायरलेस डिवाइस के संयोजन में, भविष्य के नैदानिक अध्ययनों में उपयोग किए जा सकते हैं जिनके लिए वास्तविक समय और दीर्घकालिक ईसीजी निगरानी की आवश्यकता होती है। जैल का उपयोग किए बिना या लंबे समय तक पहनने के बाद असुविधा पैदा किए बिना नैदानिक-गुणवत्ता ईसीजी रिकॉर्डिंग के लिए काफी कम इलेक्ट्रोड-त्वचा प्रतिबाधा के साथ हमने तुलनात्मक प्रदर्शन हासिल किया।

अगला काम विशेष प्रकार के नैनोकम्पोजिट उपचारित वस्त्र आधारित शुष्क बायोपोटेंशियल इलेक्ट्रोड प्रस्तुत करता है जिन्हें दीर्घकालिक ईसीजी निगरानी के लिए प्रस्तुत किया गया है। पहनने योग्य कपड़ा इलेक्ट्रोड द्वारा बनाए गए बायोपोटेंशियल सेंसिंग के लिए सूखे इलेक्ट्रोड गीले और धातु इलेक्ट्रोड की कमियों को दूर करने के लिए आराम के संदर्भ में दीर्घकालिक स्वास्थ्य निगरानी के लिए उम्मीदवारों का वादा कर रहे हैं। इस कार्य में, ईसीजी निगरानी के लिए सूखे इलेक्ट्रोड के रूप में उपयोग के लिए तीन प्रकार के कपड़ा-आधारित इलेक्ट्रोड तैयार किए जाते हैं और उनका अध्ययन किया जाता है। पहला कपड़ा इलेक्ट्रोड पॉली (3,4-एथिलीन डाइऑक्सीथियोफेन) (पेडॉट): : पॉली (स्टाइरीन सल्फोनेट) (पीएसएस) और डीएमएसओ द्वारा तैयार प्रवाहकीय स्याही के उपचार के माध्यम से ईसीजी निगरानी के लिए एक कपास आधारित कपड़ा सूखा इलेक्ट्रोड है ECG की निगरानी एक पोर्टेबल स्व-डिज़ाइन किए गए कम लागत वाले Arduino-आधारित डिवाइस द्वारा की जाती है और एक मानक ECG निगरानी प्रणाली द्वारा मान्य की जाती है। दूसरा कपड़ा इलेक्ट्रोड, Kevlar कपड़े पर AgNRs, PEDOT: PSS और DMSO का लेप करने से तैयार और अध्ययन किया। यह समान और उच्च विद्युत चालकता दिखाता है। इलेक्ट्रोड उच्च त्वचा संगतता और अच्छी सिग्नल गुणवत्ता प्रदान करता है, जो कार्डियोरेस्पिरेटरी मॉनिटरिंग के लिए प्रमुख हैं। तीसरा टेक्सटाइल इलेक्ट्रोड, लंबी अवधि के ईसीजी मॉनिटरिंग के लिए PEDOT:PSS कोटेड लेजर-प्रेरित ग्राफीन (LIG) Kevlar टेक्सटाइल ड्राई इलेक्ट्रोड। यहाँ LIG Kevlar के उत्पादन के लिए Kevlar टेक्सटाइल पर लेजर-प्रेरित ग्राफीन (LIG) के प्रत्यक्ष लेखन का उपयोग किया गया था। यह संरचना पहनने के आराम को बनाए रखते हुए वस्त्र में कार्यों को शामिल करने में सक्षम बनाती है। यथा-तैयार इलेक्ट्रोड में 40 Hz से 1 kHz तक की आवृत्तियों के लिए  $100 \pm 3 \text{ k}\Omega$  (40 Hz पर) से  $7.9 \pm 3.7 \text{ k}\Omega$  की उच्च विद्युत चालकता और त्वचा संपर्क प्रतिबाधा है, जो कि अधिकांश पारंपरिक Ag/AgCl से लगभग 13% कम है। परिणाम नैदानिक गुणवत्ता के लिए काफी कम इलेक्ट्रोड-त्वचा प्रतिबाधा के साथ तुलनीय प्रदर्शन दिखाते हैं। कई घंटों के उपयोग के बाद भी, ये इलेक्ट्रोड त्वचा में जलन पैदा नहीं करते हैं और त्वचा की तैयारी की आवश्यकता के बिना प्रभावी ढंग से काम करते हैं।

PEDOT: PSS-ग्राफीन / Kevlar टेक्सटाइल इलेक्ट्रोड का निर्माण सरल और सस्ता है, और इसे किसी भी जटिल या समय लेने वाली प्रक्रियाओं की आवश्यकता के बिना बड़े पैमाने पर उत्पादित किया जा सकता है, जो इस दृष्टिकोण के व्यावहारिक अनुप्रयोगों को लाभान्वित करता है।

निम्नलिखित कार्य नैनो इंडेंटेशन का उपयोग करते हुए AgNRs एम्बेडेड पॉलिमर मैट्रिक्स और ज़िरकोनिया ( $ZrO_2$ ) पतली फिल्मों जैसे नैनो संरचनात्मक सामग्रियों के नैनोमैकेनिकल गुणों के निर्माण और अध्ययन का वर्णन करता है। यहाँ PDMS बहुलक मैट्रिक्स के गुणों पर AgNRs के प्रभाव का अध्ययन किया गया। इसमें AgNRs एम्बेड करने के बाद PDMS की सतह, यांत्रिक और विद्युत गुणों में काफी बदलाव आया है। परिणाम बताते हैं कि AgNRs के PDMS मैट्रिक्स में एम्बेडेड होने के बाद सतह खुरदरापन और ध्रुवीयता बढ़ जाती है। इंडेंटेशन गहराई प्रभाव के परिणामस्वरूप इंडेंटेशन लोड में वृद्धि के साथ elastic मॉड्यूलस (E) और hardness (H) घट जाती है। PDMS मैट्रिक्स में एम्बेडेड AgNRs के मजबूत इंटरफेशियल आसंजन के कारण, PDMS फिल्म की तुलना में क्रमशः नैनोकम्पोजिट के E और H में 167.6% और 93.3% की वृद्धि हुई है। यह झुकने, घुमाने और खींचने जैसे विभिन्न यांत्रिक तनावों के दौरान प्रवाहकीय रहता है, जिसे प्रकाश उत्सर्जक डायोड सर्किट का उपयोग करके प्रदर्शित किया जाता है। इसके साथ ही, चांदी की रोगाणुरोधी गतिविधि इसे पहनने योग्य इलेक्ट्रॉनिक्स के लिए एक आशाजनक उम्मीदवार बना सकती है। परिणाम बताते हैं कि विद्युत संचालन और यंत्रवत् रूप से विश्वसनीय AgNRs-PDMS सम्मिश्र में स्ट्रेचेबल इलेक्ट्रोड के रूप में उपयोग किए जाने की क्षमता हो सकती है। इसके अलावा, ज़िरकोनिया पतली फिल्म को ई-बीम वाष्पीकरण तकनीक का उपयोग करके जमा किया गया था, जिसके बाद क्यूबिक चरण को अनुकूलित करने के लिए थर्मल एनीलिंग किया गया था। यह कार्य ज़िरकोनिया फिल्म के विभिन्न गुणों जैसे संरचनात्मक, ऑप्टिकल, गीला और यांत्रिक गुणों पर तापमान के प्रभाव का व्यवस्थित रूप से विश्लेषण करता है। नैनोइंडेंटेशन के परिणाम निक्षेपित फिल्म के यांत्रिक गुणों पर एनीलिंग तापमान के प्रभाव को प्रदर्शित करते हैं। एनीलिंग तापमान में वृद्धि के साथ कठोरता और लोचदार मापांक में वृद्धि हुई। 500 डिग्री सेल्सियस पर एनील की गई ज़िरकोनिया फिल्म में घन चरण, बड़े grain का आकार, उच्चतम ऑप्टिकल संप्रेषण, हाइड्रोफिलिसिटी, कठोरता और लोचदार मापांक था। नतीजतन, एनीलिंग के बाद का तापमान ज़िरकोनिया फिल्म की विशेषताओं को दृढ़ता से प्रभावित करता है, जो ज़िरकोनिया फिल्म के ऑप्टिकल, गीला और यांत्रिक गुणों को ट्यून करने के लिए एक विधि प्रदान कर सकता है।

आगे के काम में, AgNRs-कोटेड टेक्सटाइल और टेक्सटाइल एपॉक्सी कंपोजिट के नैनोमैकेनिकल गुणों की जांच की गई है। Ag नैनोरोड्स को पैरा-एरीमिड (Kevlar) फाइबर की सतह पर ग्लॉसिंग एंगल डिपोजिशन तकनीक का उपयोग करके उगाया गया था। AgNRs अंतर-यार्न घर्षण को बढ़ाते हैं, जो ऊर्जा अवशोषण अनुप्रयोगों के लिए महत्वपूर्ण मापदंडों में से एक है और इसका उपयोग हल्के, नरम शरीर कवच के लिए किया जा सकता है। कपड़े के लचीलेपन पर नैनोवायरों

का न्यूनतम प्रभाव पड़ता है, और कपड़े में जोड़े गए अतिरिक्त वजन की मात्रा नगण्य होती है। इसके अलावा, केवलर-एपाँकसी कंपोजिट की यांत्रिक विशेषताओं पर एजी नैनोरोड्स के प्रभाव का पता लगाया गया है। इसके बाद, इन हाइब्रिड सम्मिश्रणों को तन्यता, वंक और कम-वेग प्रभाव परीक्षणों के अधीन किया जाता है, और उनके प्रदर्शन की तुलना सीधे मूल केवलर-एपाँकसी सम्मिश्रण से की जाती है। AgNRs-उपचारित Kevlar कंपोजिट को इंटरलामिनर और इंटरफेशियल विशेषताओं को बढ़ाने के लिए दिखाया गया है। हमारे निष्कर्ष विभिन्न प्रकार के नैनोकम्पोजिट्स के निर्माण और अध्ययन के लिए वादा करते हैं।

## **Table of Contents**

Certificate .....	i
Acknowledgments .....	ii
Abstract .....	v
List of Figures .....	xv
List of Tables.....	xv
List of Symbols and Abbreviations .....	xxvi
<b>Chapter1: Introduction.....</b>	<b>1</b>
1.1 Composites and nanocomposites materials: An overview	2
1.2 Biopotentials and Electrocardiography	3
1.2.1 Origin of cardiac potential and ECG signal	3
1.3 Biopotential sensors	8
1.3.1 Contact surface electrodes	11
1.3.2 Polymer-based biopotential electrodes	11
1.3.3 Textile-based biopotential electrodes	12
1.3.4 Tattoo electrodes	13
1.3.5 Contact penetrating electrodes	14
1.3.6 Noncontact capacitive electrodes	15
1.4 Mechanical properties of materials	16
1.4.1 Stress and Strain	17
1.4.2 Elasticity and Plasticity	18
1.4.3 Hardness	19
1.4.4 Stiffness	20
1.4.5 Tensile strength	19
1.4.6 Flexural strength	20
1.4.7 Impact strength	21
1.5 Objectives of the thesis	22
1.6 Thesis organization	23

## **Chapter2: Experimental techniques .....25**

2.1	Fabrication techniques	26
2.1.1	Glancing angle deposition system (GLAD)	26
2.1.2	E beam evaporation system	27
2.1.3	Laser writing	28
2.2	Biopotential electrodes designing	29
2.2.1	AgNRs-PDMS-based dry electrodes	29
2.2.2	Ag/RGO-PDMS based dry electrodes	31
2.2.3	PEDOT: PSS-treated cotton-based dry electrodes	32
2.2.4	AgNRs-PEDOT: PSS treated Kevlar based dry electrodes	32
2.2.5	PEDOT: PSS-treated laser-induced graphene (LIG) based dry electrodes	34
2.3	Circuit designing for ECG monitoring	35
2.4	Characterization techniques	36
2.4.1	Electron microscopy (SEM)	36
2.4.2	Energy Dispersive X-Ray Analysis (EDX)	37
2.4.3	X-ray diffraction (XRD)	38
2.4.4	Atomic Force Microscopy (AFM)	39
2.4.5	Contact angle measurements	40
2.4.6	Raman spectroscopy	41
2.4.7	Photoluminescence (PL) measurements	42
2.5	Measurements	42
2.5.1	Biopotential measurements (ECG)	42
2.5.2	Impedance measurements	46
2.5.3	Nanoindentation	46
2.5.4	Yarn pull-out test	49
2.5.5	Tensile test	50
2.5.6	Three-point bending flexural test	51

2.5.7 Impact test	52
-------------------	----

**Chapter3: Study of AgNRs embedded polymer nano composite-based biopotential dry electrodes .....54**

3.1	Introduction	55
3.2	AgNRs embedded polydimethylsiloxane (PDMS) dry electrode	57
3.2.1	Sample fabrication	57
3.2.2	Morphology analysis of AgNRs	57
3.2.3	Morphology analysis of AgNRs-PDMS electrodes	58
3.2.4	Surface chemistry	60
3.2.5	ECG electrode evaluation test	61
3.2.5.1	Skin-to-electrode impedance measurements	61
3.2.5.2	Skin compatibility test	64
3.2.5.3	Proposed system evaluation	64
3.3	AgNRs embedded RGO-PDMS dry electrode	66
3.3.1	Sample fabrication	66
3.3.2	Morphology analysis	66
3.3.3	ECG electrode evaluation test	67
3.4	Conclusions	69

**Chapter4: Study of textile-based biopotential dry electrodes .....70**

4.1	Introduction	71
4.2	PEDOT: PSS-treated cotton-based textile electrode fabrication	72
4.2.1	Sample preparation	72
4.2.2	Chemical composition and structural analysis	72
4.2.3	ECG electrode evaluation test	74
4.3	PEDOT: PSS treated AgNRs treated Kevlar electrodes	75

4.3.1	Sample preparation	75
4.3.2	Chemical composition and structural analysis	75
4.3.3	ECG electrode evaluation test	77
4.3.3.1	Electrical characteristics	77
4.3.3.2	Skin-electrode contact impedance	78
4.3.3.3	Skin irritation test	80
4.3.3.4	ECG measurements	80
4.4	PEDOT: PSS-treated laser-induced graphene Kevlar electrodes	82
4.4.1	Sample preparation	82
4.4.2	Chemical composition and structural analysis	82
4.4.3	ECG electrode evaluation test	87
4.4.3.1	Electrical characteristics	87
4.4.3.1	Skin-electrode contact impedance	88
4.4.3.1	Skin irritation test	90
4.4.3.1	ECG measurements	91
4.5	Conclusions	92

**Chapter5: Nanomechanical properties of polymer-based nanocomposites and nano structural zirconia film using nanoindentation .....94**

5.1	Introduction	95
5.2	AgNRs embedded polydimethylsiloxane (PDMS) composite film	96
5.2.1	Sample fabrication	96
5.2.2	Characterization	97
5.2.3	Nanomechanical measurements	98
5.2.4	Electrical measurement	99
5.2.5	Results and discussion	99
5.2.5.1	Surface morphology	99
5.2.5.2	Investigation of Mechanical properties	99

5.2.5.3	Electrical measurements	107
5.3	Fabrication and study of Zirconium oxide (ZrO <sub>2</sub> ) thin films	109
5.3.1	Sample fabrication and stabilization of cubic zirconia	112
5.3.2	Characterization	113
5.3.3	Nanomechanical analysis	114
5.3.4	Results and discussion	114
5.3.4.1	Variation in phase and microstructures during annealing	114
5.3.4.2	Variation in optical characteristics	120
5.3.4.3	Influence of annealing on mechanical properties	124
5.4	Conclusions	129

**Chapter6: Nanomechanical properties of AgNRs-coated textiles and their composite.....131**

6.1	Introduction	132
6.2	Nanomechanical properties of AgNRs coated textiles	135
6.2.1	Sample preparation	135
6.2.2	Characterizations	135
6.2.3	Yarn-pull out test	135
6.2.4	Numerical modelling of yarn pull-out phenomenon	136
6.2.5	Inter yarn friction calculation	139
6.2.6	Results and Discussion	141
6.2.6.1	Morphological and structural analysis	141
6.2.6.2	Effect of AgNRs on inter-yarn friction	142
6.2.6.3	Numerical modelling	144
6.3	Nanomechanical properties of AgNRs coated textiles-epoxy composites	146
6.3.1	Preparation of Kevlar Fabric/Epoxy Composites	146
6.3.2	Morphology and Structure Analysis	147

6.3.3 Mechanical Properties analysis	147
6.3.4 Results and discussion	147
6.3.4.1 Tensile Strength	147
6.3.4.2 Flexural strength	148
6.3.4.3 Impact Resistance of composites	149
6.4 Conclusion	150
<b>Chapter7: Summary and Future Perspective.....</b>	<b>152</b>
7.1 Summary	153
7.2 Future Perspective	155
References.....	157
List of Publications.....	172
Brief Bio-Data.....	175

## List of Figures

Figure 1-1. Human heart schematic.....	4
Figure 1-2. Potential-time characteristic for heart cell due to the ion diffusion process <sup>17</sup> . .....	5
Figure 1-3. (a) Heart; conduction system, (b) human heart schematic with four-chamber and electrical nodes.....	6
Figure 1-4. ECG characteristic of a human heart. ....	7
Figure 1-5. Types of ECG electrodes. ....	9
Figure 1-6. Schematics of electrode–skin interface models for (a) wet (gel) electrode. Dry electrodes, (b) contact surface electrode, (c) contact penetrating electrode, and (d) noncontact capacitive electrode. ....	10
Figure 1-7. Typical stress-strain curve.....	18
Figure 1-8. Typical flexural load-displacement curves. ....	21
Figure 2-1. (a) Schematic of glancing angle deposition system. (b) Schematic of GLAD growth process: (i) incident vapor flux arriving at angle $\alpha$ and initial nucleation on substrate surface (ii) nuclei growth and form shadowed region (iii) columns growth started (iv) columns grow at an inclined angle $\beta$ . ....	27
Figure 2-2. Photograph of glancing angle deposition (GLAD) system. ....	27
Figure 2-3. Schematic diagram of electron beam deposition system. ....	28
Figure 2-4. Photograph of laser cutting machine.....	29
Figure 2-5. (a) The fabrication process of self-adhesive Ag nanorods embedded PDMS (AgNRs-PDMS) electrode. (b) optical images of the fabrication process of AgNRs- PDMS electrode. ....	30
Figure 2-6. (a-g) Schematic of the fabrication process of Ag nanorods embedded RGO- PDMS (AgNRs/RGO-PDMS) electrode (h) optical images of fabricated AgNRs/RGO-PDMS dry electrode.....	32

Figure 2-7. (a-c) Schematic of the fabrication process of PEDOT: PSS treated cotton-based dry electrode (d) optical images of the fabricated dry electrode. ....	32
Figure 2-8. Schematic of the electrode fabrication process (a) bare Kevlar fabric (b) AgNRs fabrication on Kevlar fabric using glancing angle deposition (c) optical image of AgNRs treated Kevlar fabric (d) components of the conductive solution (f) conductive solution treatment on AgNRs treated Kevlar, and (g) PEDOT: PSS-AgNRs treated Kevlar dry electrode.....	33
Figure 2-9. Schematic of the fabrication process of graphene on a Kevlar fabric fabricated by laser writing. (a) bare Kevlar fabric, (b) laser treatment on Kevlar fabric, (c) laser-induced graphene (LIG) on Kevlar fabric, (d) SEM image of laser-induced graphene, (e) components of conductive solution, (f) conductive solution treatment on LIG Kevlar, and (g) PEDOT: PSS-LIG treated Kevlar dry electrode. ....	35
Figure 2-10. Schematic of circuit and components used in the ECG monitoring system.	35
Figure 2-11. Optical images of the ECG monitoring unit. ....	36
Figure 2-12. Schematic diagram of scanning electron microscope & Flow chart of working Principle of SEM.....	37
Figure 2-13. Schematic of XRD Analysis. ....	39
Figure 2-14. (a) Schematic diagram and (b) Photograph of the atomic force microscope (AFM). ....	40
Figure 2-15. (a) Schematic diagram and (b) photograph of the contact angle measurement setup. ....	41
Figure 2-16. (a) Schematic of a bipolar lead system for measuring cardiac potential in the human body, (b) representation of Einthoven's triangle in the human torso; the heart vector's ( $H$ ) projection on the limb leads can be estimated from the voltage recording at bipolar limb leads (c) location of Wilson central terminal (WCT) in the human body.....	45

Figure 2-17. (a) Optical image of ECG monitoring system and placement of electrodes during ECG measurements. ....	46
Figure 2-18. (a) Schematic of nanoindentation setup (b) representation of load vs. depth graph from nanoindentation test using Berkovich tip.....	49
Figure 2-19. Photograph of nanoindentation setup equipped with ultra-nano hardness tester and optical microscope. ....	49
Figure 2-20. (a) Schematic of single yarn pull-out test (b) arrangement of the testing setup for yarn pull-out test.....	50
Figure 2-21. (a) schematic diagram of the tensile test and (b) photograph of the tensile test setup. ....	51
Figure 2-22. (a) schematic diagram of the flexural test and (b) photograph of the flexural test setup.....	52
Figure 2-23. (a) schematic diagram of impact test and (b) photograph of impact test setup. ....	53
Figure 3-1 (a, b) SEM images of as-prepared AgNRs on Si substrates (c) EDX of AgNRs on Si wafer and (d) X-ray diffraction (XRD) pattern of Ag nanorods grown by glancing angle deposition. ....	58
Figure 3-2. SEM images of as-prepared (a) PDMS film and (b) AgNRs embedded PDMS (AgNRs-PDMS) film. AFM images of (c) PDMS film and (d) AgNRs-PDMS film. Insets show 3D view for $1 \times 1 \mu\text{m}^2$ scan area.....	59
Figure 3-3. Scotch tape peel test of AgNRs embedded PDMS (a) before use (0h) and (b) after 48 h of usage (c) Fourier transform infrared (FTIR) spectrum of PDMS and AgNRs-PDMS. ....	60
Figure 3-4. Fourier transform infrared spectroscopy (FTIR) spectra of PDMS and AgNRs embedded PDMS (AgNRs-PDMS) films. ....	61
Figure 3-5. Equivalent circuit model of skin-electrode interface for (a) Ag/AgCl wet and (b) AgNRs-PDMS dry electrodes. (c) The variation of contact impedance of Al	

metal electrode, conventional Ag/AgCl wet electrode, and AgNRs-PDMS dry electrode with frequency.....	62
Figure 3-6. Variation of impedance as a function of (a) distance between the two electrodes (inset: Photograph of electrodes placed on the forearm) and (b) time for dry AgNRs-PDMS as well as wet Ag/AgCl electrodes. (c) Graph showing the variation of impedance as a function of signal frequency before and after applying the sweat-like salt solution on the skin for both dry AgNRs-PDMS and wet Ag/AgCl electrodes. (d) Skin compatibility test for 48 h of usage. Photographs show (i) the electrodes placed on the forearm, (ii) skin under the AgNRs-PDMS electrode, and (iii-iv) skin under the Ag/AgCl electrode. ....	63
Figure 3-7. ECG signal using (a) Ag/AgCl wet electrodes, (b) ECG signal using AgNRs-PDMS dry electrodes, and (c) Enlarged view of ECG signal acquired using AgNRs embedded PDMS electrodes and Ag/AgCl wet electrodes.....	65
Figure 3-8. (a-b) Screenshots of ECG monitoring using AgNRs-PDMS electrodes on the designed smartphone-based application screen. ....	65
Figure 3-9. (a) SEM image of AgNRs on Si substrate, and(b) AgNRs/RGO-PDMS surface (c) XRD and (d) Raman spectra of fabricated samples. ....	67
Figure 3-10. (a) electrical conductivity illustration, and (b) resistance measurements of fabricated AgNRs/RGO-PDMS electrode. ....	68
Figure 3-11. Equivalent circuit model of skin-electrode interface for (a) Ag/AgCl wet, (b) AgNRs/RGO-PDMS dry electrode. (c) variation of contact impedance of conventional Ag/AgCl wet electrode and AgNRs/RGO-PDMS dry electrode with frequency.....	68
Figure 3-12. ECG signal using (a) Ag/AgCl wet electrodes, (b) AgNRs/RGO-PDMS dry electrodes, and (c) Enlarged view of ECG signal acquired using Ag/AgCl wet and fabricated dry electrodes. ....	69
Figure 4-1. FE-SEM image of (a-c) untreated cotton fabric (d-f) PEDOT: PSS treated cotton fabric. ....	73

Figure 4-2. EDX spectra and elemental mapping of (a) untreated cotton fabric (b) PEDOT: PSS treated cotton fabric.....	73
Figure 4-3. (a) resistance of PEDOT: PSS treated cotton fabric by resistance meter (c-d) electrical conductivity of PEDOT: PSS treated cotton fabric illustrated using the LED circuit.....	74
Figure 4-4. ECG measurements using PEDOT: PSS treated cotton based dry electrode (a, b) by designed Arduino based circuit (c, d) by standard ECG monitoring machine. ....	75
Figure 4-5. SEM image of (a-d) AgNRs grown on the Kevlar fabric for the different magnification (e) PEDOT: PSS treated AgNRs Kevlar fabric surface.....	76
Figure 4-6. (a) XRD pattern Kevlar fabric before and after AgNRs deposition. (b) EDX spectrum of Kevlar fabric after Ag nanorods deposition.....	77
Figure 4-7. Resistance of (a) bare, (b) AgNRs deposited Kevlar fabric, and (c) PEDOT: PSS treated AgNRs Kevlar fabric. (c, d, e) electrical behaviour of bare, AgNRs deposited Kevlar and PEDOT: PSS treated AgNRs-Kevlar illustrated using the LED circuit.....	78
Figure 4-8. The electronic representation of the interface of skin and electrode for (a) wet electrode and (b) PEDOT: PSS-AgNRs Kevlar dry textile electrodes. (c) Variation of contact impedance for wet electrode, AgNRs deposited Kevlar, and PEDOT: PSS-AgNRs Kevlar dry textile electrodes with frequency. ....	79
Figure 4-9. (a) Variation of impedance as a function of time for dry PEDOT: PSS-AgNRs treated Kevlar dry electrode and wet Ag/AgCl electrodes. (b) Skin reaction comparison for 48 h of usage. Photographs show (i) electrode placement, (ii) skin condition under the conventional wet electrode, and (iii) skin under the PEDOT: PSS-AgNRs treated Kevlar dry electrode.....	80
Figure 4-10. (a, b) Optical image of ECG monitoring system and placement of electrodes during ECG measurements (c) Zoom view of ECG signal obtained using PEDOT: PSS-LIG treated Kevlar dry electrode and Ag/AgCl wet electrodes. ECG signal	

recorded using (c) wet electrodes and (d) proposed PEDOT: PSS-AgNRs treated Kevlar dry electrodes. ....	81
Figure 4-11. SEM image of (a-c) bare Kevlar fabric (d-f) laser-induced treated (LIG) Kevlar fabric (g-i) PEDOT: PSS treated LIG Kevlar fabric surfaces for the different magnification. ....	83
Figure 4-12. (a) Raman spectra of the LIG and bare Kevlar fabric. (b) XRD spectra for bare Kevlar, LIG, PEDOT: PSS solution, and PEDOT-PSS-LIG treated Kevlar fabric. ....	84
Figure 4-13. TEM image of the laser-induced graphene from Kevlar. The average lattice space is $\sim 0.34$ nm, which is consistent with the distance between neighboring (002) planes in few-layer graphene. (f) Selective area electron diffraction (SAED) pattern derived from (b). ....	85
Figure 4-14. EDX spectra and elemental mapping of (a) LIG Kevlar and (b) PEDOT: PSS treated LIG Kevlar. ....	86
Figure 4-15. Schematic illustration of the graphene formation on Kevlar fabric surface by laser-writing (a) bare Kevlar fabric (b) chemical structure of Kevlar fabric (b) transformation of Kevlar to laser-induced laser graphene (LIG). ....	87
Figure 4-16. Resistance of (a) bare, (b) LIG and (c) PEDOT: PSS treated Kevlar, (c, d, e) electrical behavior of bare, LIG, and PEDOT: PSS treated Kevlar illustrated using the LED circuit. ....	88
Figure 4-17. The electronic representation of the interface of skin and electrode for (a) wet electrode and (b) dry textile electrodes. (c) Variation of contact impedance for wet electrode, LIG treated Kevlar, and PEDOT: PSS-LIG treated Kevlar dry electrode with frequency. ....	89
Figure 4-18. (a) Variation of impedance as a function of time for dry PEDOT: PSS-LIG treated Kevlar dry electrode and wet Ag/AgCl electrodes. (b) Skin reaction comparison for 48 h of usage. Photographs show (i) electrode placement, (ii) skin	

condition under the PEDOT: PSS-LIG treated Kevlar dry electrode, and (iii) skin under the PEDOT: PSS-LIG treated Kevlar dry electrode. ....	90
Figure 4-19. (a) Optical image of ECG monitoring system and placement of electrodes during ECG measurements (b) Zoom view of ECG signal obtained using PEDOT: PSS-LIG treated Kevlar dry electrode and Ag/AgCl wet electrodes. ECG signal recorded using (c) wet electrodes and (d) proposed dry electrodes.....	92
Figure 5-1. Schematic showing the steps of fabrication (a) PDMS film and (b) Ag nanorods embedded PDMS (AgNRs-PDMS) film. (c) optical images of the peeling process for AgNRs-PDMS film.....	97
Figure 5-2. Load–displacement (P-h) curves for PDMS and AgNRs- PDMS film with Berkovich indenter, up to different maximum load ( $P_m$ ) values of (a) 30 $\mu\text{N}$ (b) 50 $\mu\text{N}$ (c) 150 $\mu\text{N}$ (d) 150 $\mu\text{N}$ and (e) 200 $\mu\text{N}$ , respectively.....	100
Figure 5-3. The variation of (a) maximum penetration depth, (b) elastic modulus ( $E$ ), and (c) hardness ( $H$ ), for PDMS and AgNRs- PDMS films for 30, 50, 100, 150, and 200 $\mu\text{N}$ loads. ....	102
Figure 5-4. AFM images of an indent created by applying (a) 50 $\mu\text{N}$ and (b) 200 $\mu\text{N}$ using Berkovich tip on AgNRs-PDMS film.....	102
Figure 5-5. Dynamic indentation or sinus mode nanoindentation: (a) Dynamic calibration of ultra-nano hardness tester (UNHT) head, (b) the dynamic force-time curve for a normal force of 500 $\mu\text{N}$ using an oscillatory frequency of 10 Hz; inset graph shows the zoom view of force signal, which is superimposed by the small amplitude of oscillation, (c) dynamic force-penetration depth (P-h) curve, and (d) stiffness as a function of penetration depth for PDMS and AgNRs-PDMS film (light background shows X and Y errors). ....	103
Figure 5-6. Variation of (a) elastic modulus ( $E$ ), (b) hardness ( $H$ ), (c) storage modulus ( $E'$ ), and (d) loss modulus ( $E''$ ) as a function of dynamic penetration depth with a normal force of 500 $\mu\text{N}$ using an oscillatory frequency of 10 Hz for PDMS and AgNRs-PDMS films. ....	106

Figure 5-7. Variation of (a)  $\tan \delta$  as a function of dynamic penetration depth with a normal force of 500  $\mu\text{N}$  using an oscillatory frequency of 10 Hz for PDMS and AgNRs-PDMS films (b) current-voltage (I-V) characteristic curve of AgNRs-PDMS film. ....107

Figure 5-8. The AgNRs-PDMS electrodes with reliable mechanical and electrical characteristics under various mechanical deformation conditions (a) unstretched state, (b) under bending strain, (c-d) under twisting conditions, (e) circuit diagram. ....108

Figure 5-9. Photographs of a light-emitting diode (LED) operating in conjunction with AgNRs- PDMS electrodes under strain values of (a) 0, (b) 20, (c) 40, (d) 60, (e) 80, and (f) 90%. ....109

Figure 5-10. Schematic of the fabrication process of zirconium film using e-beam deposition system followed by thermal annealing (a) e-beam deposition system (b) thermal annealing in the furnace (c)  $\text{ZrO}_2$  deposition on Si or glass substrate using e-beam (d) annealed zirconia sample.....113

Figure 5-11 X-Ray diffraction (XRD) patterns for S1\_RT, S2\_200, S3\_300, and S4\_500 zirconia films (b) XRD spectra for  $2\theta$  values for S4 film for  $70^\circ$  to  $80^\circ$ , (c) simulated XRD pattern and (d) visualization of the cubic  $\text{ZrO}_2$  crystal structure.....116

Figure 5-12. (a) Raman Spectra for S1\_RT, S2\_200, S3\_300, and S4\_500 zirconia films, the red arrow indicates the characteristic cubic phase peak. (b) The zoom view of the characteristic of the cubic phase for S4\_500 film.....117

Figure 5-13. SEM images (a) S1\_RT (inset: cross-section of zirconia film as deposited, the red line shows the 500 nm thickness of the deposited film), (b) S2\_200 (c) S3\_300 (d)S4\_500 of deposited zirconia film.....118

Figure 5-14. (a-b) EDX elemental mapping images and (c) elemental spectra for S4\_500 zirconia film. ....119

Figure 5-15. AFM images of zirconia film (a) S1\_RT, (b) S2\_200, (c) S3\_300, and S4\_500. ....120

Figure 5-16. (a) UV-Visible spectra of as-deposited and annealed zirconia films (b) optical images of zirconia films on glass at RT and annealed at 500°C. ....	121
Figure 5-17. (a) UV-Vis absorption spectra and (b) Tauc plot of the as-deposited and annealed zirconia films. ....	122
Figure 5-18. (a) The full spectrum scan of XPS (b) the fine spectra of Zr 3d, and (c) O 1 s for ZrO <sub>2</sub> film deposited on Si (100) annealed at 500 °C. ....	123
Figure 5-19. (a) Quasi-Static load-displacement (P-h) curves (b) load-time graph for static analysis variation of (c) hardness (d) elastic modulus (e) maximum penetration depth for zirconia thin film annealed at different temperatures. ....	125
Figure 5-20. Dynamic nanoindentation (a) P-h curves (b) load-time graph (inset: sinusoidal component to a quasi-static load using an oscillation frequency of 10 Hz). ....	126
Figure 5-21. Variation of (a) sinus-hardness, (b) sinus- elastic modulus, and (c) contact stiffness for zirconia thin film annealed at different temperatures. ....	128
Figure 6-1. Schematic of yarn pull-out geometry for AgNRs coated Kevlar fiber during yarn pull-out test (a) AgNRs-1 sample geometry (b) AgNRs-2 sample geometry. ....	136
Figure 6-2. (a) SEM image of cross-section of single yarn (b) detailed illustration of single yarn showing its geometrical parameters width (0.5 mm, wavelength (1 ± 0.01 mm), and thickness (0.15 mm). ....	137
Figure 6-3. (a) Mesoscale level numerical model for yarn pull-out simulation. Yarns are fixed at the bottom except the yarn to be pulled (b) Single yarn movement in the mesoscale level numerical model during yarn pull-out phenomenon. ....	139
Figure 6-4. (a, b) Schematic representation of capstan test setup to calibrate yarn surface friction and (c) capstan test setup to calibrate yarn surface friction. ....	141
Figure 6-5. Optical images of Kevlar fabric(a) before and (b) after deposition of Ag nanorods on it (inset: (SEM images) ....	142

Figure 6-6. (a) Schematic illustration of the yarn pull-out mechanism (b) yarn pull-out, force-displacement curve for during yarn pull-out testing (c) yarn pull-out test results (c) yarn pull-out force (d) yarn pull-out energy for neat and treated Kevlar fabrics.....143

Figure 6-7. (a) Yarn pull-out force variation with yarn displacement for different values of COF ( $\mu$ ) (b) peak yarn pulls out values at different values of COF ( $\mu$ ). .....145

Figure 6-8. A schematic diagram of Kevlar epoxy and AgNRs treated Kevlar epoxy composites fabrication procedure. ....147

Figure 6-9. Optical image of tensile test samples (a) bare Kevlar-epoxy composite (b) AgNRs treated Kevlar epoxy composite. (c) Tensile test results for the tested bare Kevlar epoxy and AgNRs treated Kevlar epoxy composites.....148

Figure 6-10. Optical image of flexural test samples (a) bare Kevlar-epoxy composite (b) AgNRs treated Kevlar epoxy composite. (c) flexural test results of the tested bare Kevlar epoxy and AgNRs-treated Kevlar epoxy composites. ....149

Figure 6-11. Optical image of impact test samples (a) bare Kevlar-epoxy composite (b) AgNRs treated Kevlar epoxy composite (b, c) Impact test results for the tested bare Kevlar epoxy and AgNRs treated Kevlar epoxy composites.....150

## List of Tables

Table 1-1 Flexible dry contact surface electrodes comparison.....	13
Table 3-1. Impedance measurement as a function of the distance between two electrodes and usage time.....	64
Table 5-1.Variation of mechanical properties for zirconia thin film annealed at different temperatures.....	129
Table 6-1.Material properties of yarn incorporated in numerical studies.....	137
Table 6-2. Yarn pull-out force- and pull-out energy values for the neat and treated Kevlar fabrics for single yarn pull-out test. ....	145

## List of Symbols and Abbreviations

### Symbols

$\alpha$	Azimuthal angle
A	Area
$C_s$	Loss stiffness
$E_g$	Bandgap
E	Elastic modulus
$E_r$	Reduced modulus
$E'$	Storage modulus
$E''$	Loss modulus
H	Hardness
$h_c$	Contact depth
i	Indenter
$k_s$	Storage stiffness
$\omega$	Loading frequency
$\nu$	Poisson's ratio
$P_{max}$	peak load

### Abbreviations

AFM	Atomic Force Microscopy
AgNRs	Silver nanorods
AV	Atrioventricular
CA	Contact angle
CVD	Chemical Vapor Deposition
CVDs	Cardiovascular diseases
DI	Deionized
DMSO	Dimethyl sulfoxide
ECG	Electrocardiography
EDX	Energy dispersive X-ray spectroscopy
FE	Field Emission
GLAD	Glancing angle deposition system
IPA	Isopropyl alcohol
I-V	Current-Voltage
LEDs	Light Emitting Diodes
LIG	Laser-induced graphene
PEDOT: PSS	Poly(3,4-ethylenedioxythiophene): Poly (styrene sulfonate)
PDMS	polydimethylsiloxane
PVD	Physical vapor deposition
PL	Photoluminescence
RGO	Reduced graphene oxide
RMS	Root mean square
RT	Room temperature

SA	Sinoatrial
SC	Stratum corneum
SNR	Signal-to-noise ratio
SEM	Scanning electron microscope
S-NI	Sinus mode nanoindentation
UNHT	Ultra-nano hardness tester
UV	Ultraviolet
XRD	X-ray diffraction